

## Article

# Conversion Study on the Formation of Mechanochemically Synthesized BaTiO<sub>3</sub>

Gábor Kozma <sup>1,\*</sup>, Kata Lipták <sup>1</sup>, Cora Deák <sup>1</sup>, Andrea Rónavári <sup>1</sup>, Ákos Kukovecz <sup>1</sup> and Zoltán Kónya <sup>1,2</sup>

<sup>1</sup> Department of Applied and Environmental Chemistry, University of Szeged, 6720 Szeged, Hungary; liptak.katalina@gmail.com (K.L.); cora@chem.u-szeged.hu (C.D.); ronavari@chem.u-szeged.hu (A.R.); kakos@chem.u-szeged.hu (Á.K.); konya@chem.u-szeged.hu (Z.K.)

<sup>2</sup> MTA-SZTE Reaction Kinetics and Surface Chemistry Research Group, 6720 Szeged, Hungary

\* Correspondence: kozmag@chem.u-szeged.hu

**Abstract:** Mechanochemistry is a method that can cover the energy demand of reaction pathways between solid materials. This requires enough energy to maintain the reactions between the starting materials. This is called “high-energy milling”. In our case, a planetary ball mill provided the required energy. Using the Burgio-equation, the required energy is determinable; the energy released during a single impact of a milling ball ( $E_b$ ), as well as during the whole milling process ( $E_{cum}$ ). The aim of this work was the one-step production of BaTiO<sub>3</sub> from BaO and TiO<sub>2</sub> starting materials. Whereas during mechanochemical reactions it is possible to produce nanoparticles of up to 10 nm, the essence of this study is to develop the preparation of BaTiO<sub>3</sub> with a perovskite structure even without subsequent heat treatment, since sintering at high temperatures is associated with a rapid increase in the size of the particles. By describing the synthesis parameters and their energy values ( $E_b$  and  $E_{cum}$ ), it is possible to transpose experimental conditions, so that in the case of other types of planetary ball mills or grinding vessel made of other materials, the results can be used. In this study, the mechanical treatment was carried out with a Fritsch Pulverisette-6 planetary ball mill and the transformation of the starting materials was investigated by X-ray diffractometric, Raman and Energy-dispersive X-ray spectroscopic, and transmission electron microscopic measurements.

**Keywords:** mechanochemistry; perovskite; BaTiO<sub>3</sub>; ball-milling; nanoparticles



**Citation:** Kozma, G.; Lipták, K.; Deák, C.; Rónavári, A.; Kukovecz, Á.; Kónya, Z. Conversion Study on the Formation of Mechanochemically Synthesized BaTiO<sub>3</sub>. *Chemistry* **2022**, *4*, 592–602. <https://doi.org/10.3390/chemistry4020042>

Academic Editors: Marcela Achimovičová, Matej Baláž and Abhishek Lokhande

Received: 29 April 2022

Accepted: 13 June 2022

Published: 15 June 2022

**Publisher's Note:** MDPI stays neutral with regard to jurisdictional claims in published maps and institutional affiliations.



**Copyright:** © 2022 by the authors. Licensee MDPI, Basel, Switzerland. This article is an open access article distributed under the terms and conditions of the Creative Commons Attribution (CC BY) license (<https://creativecommons.org/licenses/by/4.0/>).

## 1. Introduction

Ceramics are produced and used in huge quantities all over the world due to the wide variety of probable applications. In total, there are only a few minerals with applications and technological uses that dominate the industrial application (e.g., quartz, calcium silicates, alumina, and titanium dioxide). These materials are characterized by both the crystal structure and the composition and are important due to their specific properties and applications. The question arose whether there is a structure that is multifunctional and crystallographically suitable for the development of useful properties. Considering the three-component crystal structures, there are only a dozen ceramics that are widely used. Among them, the A<sub>2</sub>BX<sub>4</sub> spinel and ABX<sub>3</sub> perovskite excel and perovskite is the only structure, the chemical modification of which results in an extremely wide range of phases with completely different properties [1]. Due to its unique electrical properties, the family of chemical compounds with perovskite-structure permits a wide range of electrotechnical applications: semiconductor dielectrics, superionic conductors, combined with ionic and electron conductivity for high-temperature superconductors [2].

The possibility of fine grinding, mechanical activations and chemical reactions that can be carried out in planetary ball mills has long been known. However, several factors affect the success of each milling, since the energy generated during milling must be in balance with the properties of the desired product, therefore predetermined, optimal parameters

are very important. It is necessary to consider the material quality of the grinding vessel and balls; the rotational speed; the time of treatment; the applied atmosphere and temperature [3], the number of balls and the filling ratio of the balls and reactants; and the physical and chemical properties of the reactants [4]. These parameters are also very interdependent and play an important role in the development of optimal milling energy, thus achieving the best product yield in the shortest reaction time [5]. Obviously, higher milling energy can be achieved by increasing the rotational speed or using a grinding vessel of higher hardness. In our case, grinding vessels made of three different materials (silicon nitride, stainless steel, tungsten carbide) were used, although there are studies in which BaTiO<sub>3</sub> was produced in zirconia grinding vessels [6,7]. The intensity of grinding increases the particle size of crystalline materials, or when powders are ground, compounds of different compositions can be formed with a temperature change. However, it should be noted that too much energy may cause the onset of secondary reactions, such as product degradation or transformation.

In the literature, many examples can be found in the production of barium titanate from barium-oxide [8] or barium-peroxide [9] and titanium-dioxide precursors. In many of these cases, mechanical activation is used [10]. It is important to note that this does not mean the transformation of the starting materials during grinding, but is only used for the thorough mixing of precursors, while the perovskite-structured barium titanate is formed during the subsequent heat treatment [8–10]. High-energy milling may be suitable for creating the conditions for the temperature required for subsequent calcination. Research of this kind began as early as the 1960s when Bowden and Yoffe introduced the “Hot-spot” theory [11]. Later, Weicher and Schiner experimentally demonstrated that the area carrying extra energy is about 1 mm<sup>2</sup> with a temperature of 1000–1500 K, which keeps this state for about 10<sup>−4</sup>–10<sup>−3</sup> s [12]. By providing this extra energy, it is also possible to develop BaTiO<sub>3</sub> mechanochemically. It should be noted that, in addition to the mechanochemical process, BaTiO<sub>3</sub> perovskite can also be produced in several other ways, including a wet-chemical [13], hydrothermal [14], or microwave-assisted hydrothermal reaction [15]. In contrast, the mechanochemical process has the advantage that it does not require an expensive solvent, it can be produced in one step, and, as we present later, there is no need for subsequent heat treatment [16]. The advantage of this is that, it avoids the increase in the size of the particles at high temperatures and avoids the undesirable transformation of the product, which in many cases can happen even during mechanical treatment [17].

In this study, we followed the formation of perovskite-structured barium titanate from BaO and TiO<sub>2</sub> precursors with X-ray diffractometric (XRD) and Raman spectroscopic measurements. To do this, we used three grinding drums of different hardness and methodically changed the number of grinding balls, the rotational speed, and the time of grinding. Using the Energy-dispersive X-ray spectroscopic (EDS) technique, we measured the barium-titanium ratio of the powder mixture. Since BaO is water-soluble (~3.6 g/100 mL at 20 °C) as opposed to BaTiO<sub>3</sub> and TiO<sub>2</sub>, which are practically insoluble in water, after washing with distilled water the ratio of the two metals must change.

## 2. Materials and Methods

### 2.1. The Ball-Milling Experiments

The grinding was carried out in a Fritsch Pulverisette-6 planetary ball mill. Such mills are suitable for high-energy milling, which allows them to provide the energy needed to form BaTiO<sub>3</sub>. In each case, grinding balls with a diameter of 10 mm were used in the three grinding vessels (80 mL) of the same material. To produce BaTiO<sub>3</sub> 2.00 g BaO (99.99%) and 1.04 g TiO<sub>2</sub> (≥99%) were measured in all cases. The energy released during the millings has been predetermined. This was made possible by the energy model introduced by Burgio et al. [18]. The applicability of the model to our system has already been proven by our research team experimentally [19]. The Equation (1) can be used to determine two energy values: the E<sub>b</sub> (1), which represents the total energy available during an impact event of a

milling ball, and  $E_{cum}$  (2), which means the energy transferred to 1 g of the powder during the whole milling:

$$E_b = \frac{1}{2} \varphi_b K \left( \rho_b \frac{\pi d_b^3}{6} \right) \omega_p^2 \left[ \left( \frac{\omega_v}{\omega_d} \right)^2 \left( \frac{d_v - d_b}{2} \right)^2 \left( 1 - 2 \frac{\omega_v}{\omega_d} \right) - 2r_p \left( \frac{\omega_v}{\omega_d} \right) \left( \frac{d_v - d_b}{2} \right) - \left( \frac{\omega_v}{\omega_d} \right)^2 \left( \frac{d_v - d_b}{2} \right)^2 \right] \quad (1)$$

where  $K$  is the geometric constant of the mill,  $\varphi_b$  is the obstruction factor,  $\rho_b$  is the density of the milling balls,  $d_b$  is the diameter of the balls,  $d_v$  is the diameter of the grinding vessel,  $\omega_p$  and  $\omega_v$  is the rotational speed of the disc and the vessel and  $r_p$  is the distance between the rotational axes of the disc and the vessel [19].

$$E_{cum} = \frac{E_b \times f \times t}{m_p} \quad (2)$$

where  $f$  is the frequency of impacts,  $t$  is the milling time and  $m_p$  is the mass of the measured sample. Thus, it is possible to produce our product in similar energy conditions using different parameters. This answers our question as to whether the perovskite structure can be formed in all three grinding vessels. In the experiments, we changed the rotational speed from 300 to 500 rpm, the number of grinding balls from 10 to 25. In all cases, the grinding took 3 h. For XRD measurements, samples were taken hourly, while for Raman and EDS measurements 3-h samples were used.

## 2.2. Characterization

The powder X-ray diffraction patterns were obtained using a Rigaku Miniflex II XRD (Rigaku Corporation, Tokyo, Japan) instrument operating with Cu  $K\alpha$  radiation ( $\lambda = 1.5406 \text{ \AA}$ ). The  $2\theta$  Bragg angles were scanned over a range of  $5\text{--}90^\circ$  at a rate of  $1.0^\circ \text{ min}^{-1}$ . Transmission Electron Microscope (TEM) analysis was performed with a FEI Tecnai G<sup>2</sup> 20 X-TWIN instrument with a point resolution of 0.26 nm. Samples were placed on holey carbon-coated copper grids of 300 mesh. Raman characterization was performed at the excitation wavelength of 532 nm, and a nominal laser power of 12.5 mW (Senterra Bruker Optik GmbH, Ettlingen, Germany). The spectral resolution was set to ca.  $3\text{--}5 \text{ cm}^{-1}$ , and the interferometer resolution was  $1.5 \text{ cm}^{-1}$ . The elemental composition of the prepared samples was characterized by energy-dispersive X-ray spectroscopy (Hitachi Co., Tokyo, Japan) operating at 20 kV, equipped with a Röntec energy dispersive spectrometer with a 12 mm working distance. Transmission Electron Microscope (TEM) analysis was performed by an FEI-Tecnai G2/20/X-TWIN (FEI Company, Hillsboro, OR, USA) instrument with a point resolution of 0.26 nm. Samples were placed on holey carbon-coated copper grids of 300 mesh.

## 3. Results

9 different settings were determined based on the energy model. These values are shown in the table below.

It can be seen that higher density grinding vessels and rotational speed increase the value of the  $E_b$ , although there are smaller overlaps, such as SiN500/25 and stainless steel SN300/25 settings.

In the case of  $E_{cum}$  values, this increase is not so gradual, since the number of grinding balls used increases the frequency of impacts. Therefore, a higher  $E_{cum}$  may be obtained for the lower density  $\text{Si}_3\text{N}_4$  vessel, where 25 grinding balls have been inserted than for the FeNiCr vessel with a density of 2.3 times higher, where this value is lower due to slower rotation and fewer grinding balls.

Raman spectroscopic measurements were performed on all 9 samples at excitation wavelengths of 532 nm (Figure 1). On the spectra, the characteristic peaks of  $\text{TiO}_2$  and  $\text{BaTiO}_3$  are clearly observed. In the case of  $\text{TiO}_2$ , characteristic peaks of the anatase structure were observed [20].  $\text{TiO}_2$  Raman-active lattice vibrations assigned as follows: ( $A_1$ )  $516 \text{ cm}^{-1}$  + ( $B_1$ )  $636 \text{ cm}^{-1}$  + ( $B_1$ )  $395 \text{ cm}^{-1}$  + ( $E$ )  $635 \text{ cm}^{-1}$  + ( $E$ )  $144 \text{ cm}^{-1}$  + ( $E$ )  $198 \text{ cm}^{-1}$  the weak

band at  $796\text{ cm}^{-1}$  was assigned as the first overtone of the B1 mode [21]. The Raman spectrum of  $\text{BaTiO}_3$  crystals assigned as follows:  $(A_1)$   $186\text{ cm}^{-1}$  +  $(A_1)$   $265\text{ cm}^{-1}$  +  $(B_1)$   $303\text{ cm}^{-1}$  and an asymmetric broadband  $(A_1/E)$   $520\text{ cm}^{-1}$  and a broad weak peak at  $(A_1/E)$   $720\text{ cm}^{-1}$  [22]. Of the weak bands of  $\text{BaO}$ , only the most intense peak signal was detected at  $(A_1)$   $193\text{ cm}^{-1}$  [23,24]. Due to the overlap between the starting materials and the vibrations of the product, the progress of conversion cannot be clearly stated only based on the most intense peak of  $\text{BaTiO}_3$  [25]. Therefore, it is possible to deduce from the decrease in the intensity of the individual vibrations of  $\text{TiO}_2$  the re-evaluation of the precursors [26].

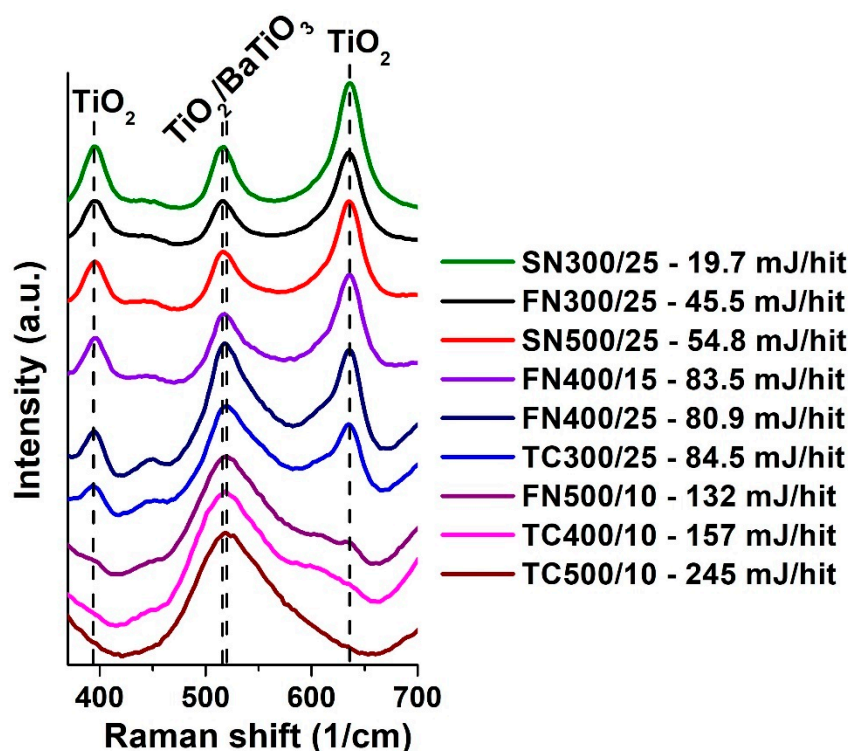


Figure 1. Raman spectra of all samples treated at different ball-impact energy ( $E_b$ ).

Figure 1 shows the Raman spectra of all samples between  $370\text{--}700\text{ 1/cm}$ . In this period there are three intensive peaks specific to  $\text{TiO}_2$  and one peak typical of  $\text{BaTiO}_3$ . The peaks of  $516$  and  $520\text{ 1/cm}$  largely overlap with each other [26]. Nevertheless, by increasing the  $E_b$ , the change in intensity at the peaks of  $\text{TiO}_2$   $395$  and  $636\text{ 1/cm}$  can be traced, which gradually disappears towards with the increasing energies. In the case of samples treated at the highest  $E_b$  (FN500/10; TC400/10; TC500/10), these peaks are barely detectable, while the peak typical of  $\text{BaTiO}_3$  in this range dominates at  $456\text{ 1/cm}$ .

The rate of transformation of starting materials is well suited to the rate of the growing  $E_b$ . The only exceptions were the FN400/15 and FN400/25 samples, where even though in the latter case the  $E_b$  was  $3.11\%$  less, the rate of transformation was slightly higher. This phenomenon can be explained by an increase in the number of grinding balls and, with it, by a higher value of  $E_{cum}$ , which was  $61.5\%$  higher in case the of the sample FN400/25 (Table 1). This is supported by previous experience: the reaction rate is basically determined by the input energy, but the frequency of impacts also counts, especially if the energy transferred may be accumulating to some extent [19].

**Table 1.** Values of  $E_{cum}$  and  $E_b$  for each grinding vessel.  $\omega_p$ : rotational speed of the grinding vessel.  $N_b$ : number of grinding balls.

Grinding Vessel	$\omega_p$ (1/s)	$N_b$ (pcs)	$E_b$ (J/hit)	$E_{cum}$ (J/g)	Short Name
$Si_3N_4$	300	25	0.0197	5907	SN300/25
	500	25	0.0548	27,350	SN500/25
FeNiCr	300	25	0.0455	13,613	FN300/25
	400	25	0.0809	32,269	FN400/25
	400	15	0.0835	19,989	FN400/15
TC	500	10	0.132	26,311	FN500/10
	300	25	0.0845	25,282	TC300/25
	400	10	0.157	25,018	TC400/10
	500	10	0.245	48,865	TC500/10

In addition to Raman spectroscopic measurements, the formation of  $BaTiO_3$  has been measured by XRD in this case of different grinding vessels (Figure 2). The typical reflections of  $BaTiO_3$  between 2 theta 20–80° are listed below: 2 theta 22.04° (100); 31.44° (110); 38.76° (111); 45.08° (200); 50.72° (210); 56.02° (211); 65.68° (220); 70.20° (300); 74.66° (310); 78.98° (311) [27].  $BaTiO_3$  produced at a sintering temperature above 1000 °C, is typically tetragonal, which is changed in hexagonal structure at 1400 °C [28]. The evolution of the starting materials and the reflections characteristic of  $BaTiO_3$  can be clearly tracked by increasing the milling energy [26]. With mechanochemical treatment, the energy required for the formation of the tetragonal structure was provided during the 3-h milling process, which was detected first in the SN500/25 sample. The  $E_b$  limit for the transformation of the precursors is therefore above 50 mJ/hit. Below this value, the perovskite structure does not form despite further 6 h of grinding. This is additional information compared to Raman results, as those measurements did not clearly show the beginning of the conversion due to the overlap of the peaks of the precursors and the product.

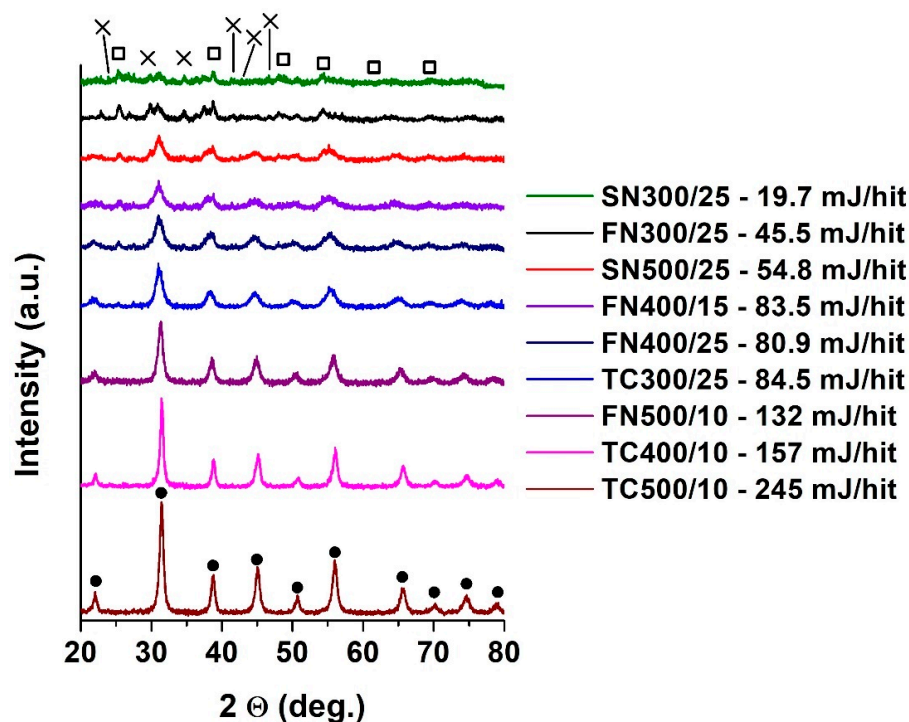


**Figure 2.** XRD diffractograms of all samples treated at different ball-impact energy ( $E_b$ ). •:  $BaTiO_3$ , □:  $TiO_2$ , ×:  $BaO$  reflections.

As in the previous results, the exchange of FN400/25 and FN400/15 samples (by the value of  $E_b$ ) based on intensities was observed in XRD measurements. This supports the hypothesis that, in addition to the appropriate  $E_b$ , sufficient treatment time ( $E_{cum}$ ) should be ensured.

For better visualization of the XRD results, diffractograms were used to track the formation of  $BaTiO_3$  product at the intensity of most typical peaks at  $2\theta$   $31.4^\circ$ , i.e., based on the fact that the intensity of this peak shows the increasing appearance of the product in the grinding vessel (Figure 3). As a result, a so-called “milling-map” was created [29]. A good correlation between the performed  $E_b$  and the reflection intensity is observed. The threshold for ball-impact energy required to produce the  $BaTiO_3$  is well-drawn, which is around 0.05 J/hit. In mechanochemistry, this is a typical limit, i.e., below  $E_b = 0.05$  J/hit low-energy, while above it is high-energy milling [29,30]. The latter arises from the limiting factor of typical single-axis mills that, when using such a mill at too high a rotational speed, the balls already move together with the walls of the grinding vessel above a certain value. In a planetary ball mill, the complex rotation determined by the two axes, up to a very high rotational speed, does not prevent the grinding balls detach and impact into the walls of the grinding vessel [31]. Low-intensity reflections will only be replaced in samples ground with the highest impact energy with signals higher than 400 cps, which clearly show the presence of tetragonal  $BaTiO_3$ .

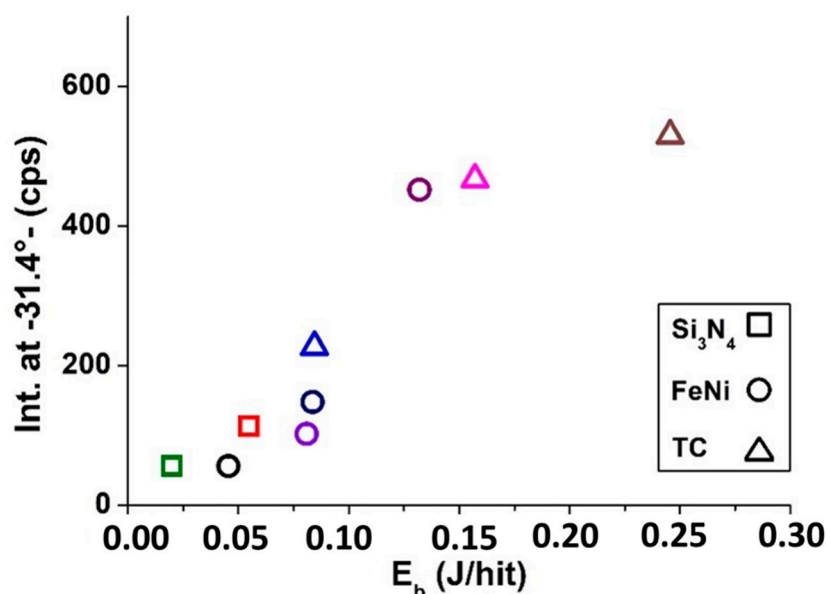


**Figure 3.** XRD measurement-based ( $BaTiO_3$  peak intensity at  $2\theta$   $31.4^\circ$ .) milling-map of  $BaTiO_3$  samples in different grinding vessels.

Based on the Raman and XRD results, the minimum  $E_b$  required for the formation of the perovskite structure can be determined ( $\sim 0.05$  J/hit). However, to be able to draw on the relationship between the  $E_b$  and  $E_{cum}$  and the amount of  $BaTiO_3$  converted, a quantification was also necessary, thus, the energy-dispersive X-ray spectrum of all 9 samples has been measured (Figure 4). Since the water solubility of  $BaO$  is  $\sim 36$  g/L at  $20^\circ C$ , assuming that the weighed 2.0 g is not converted to  $BaTiO_3$  at all, it can dissolve in a minimum of  $\sim 57$  mL of water. In comparison, to prove that all  $Ba$  present in the form of  $BaO$  has been removed, all samples have been washed with 2 L of deionized water. High-intensity characteristic peaks corresponding to  $Ba$  ( $L_a$ —4.47;  $B_{b1}$ —4.83;  $B_{b2}$ —5.17 keV) and  $Ti$  ( $K_a$ —4.50;  $K_b$ —4.91 keV) elements were noticed in the EDS patterns of the nanoparticles [32]. The percentage of  $Ba$  and  $Ti$  relative to each other was plotted from the resulting values.

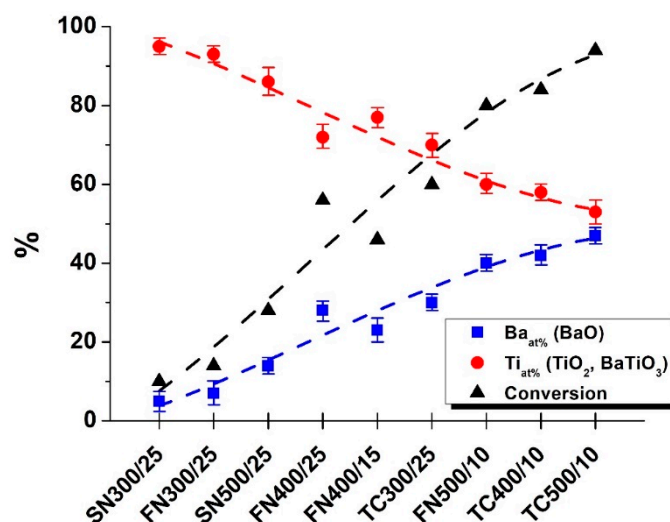


**Figure 4.** The atomic percentage (at%) of Ba (■) and Ti (●) based on EDS measurements, and the calculated conversions (▲) of the precursors. Dashed lines in the figure are guides for the eye.

Figure 4 shows the changes in the percentage distribution of the two elements examined and the calculated conversions. As the reaction progresses, the barium content of the BaO precursor is gradually integrated into the water-insoluble BaTiO<sub>3</sub>, so that its amount will increase continuously in the sample that remains after distilled water wash. The absolute amount of titanium should not change, as it is still in water-insoluble form as a precursor and after being incorporated into BaTiO<sub>3</sub>, but its relative amount will decrease in relation to barium. If all starting materials were to be converted to BaTiO<sub>3</sub>, the Ba-Ti ratios would have to be 50–50%. In the sample milled with the highest  $E_b$  and  $E_{cum}$  (TC500/10), the conversion value was 94%. Further conversion trends can be seeded from the path of the pasted curve, as it gradually saturates. The 94% value could be increased by extending the milling time, but the 100% cannot be achieved due to the trapping of the precursors (on the wall of the grinding vessel, in particular at the junction of the lid and the vessel wall) [33].

Figure 5 summarizes conversion data calculated from EDS measurements,  $E_b$  and  $E_{cum}$  values as a function of each sample. The  $E_b$  values of the samples (FN400/25, FN400/15, TC300/25) within the area framed by the dotted line are almost the same, the differences are below 5%. In  $E_{cum}$ , however, there are significant differences due to the number of grinding balls and the rotational speed. This discrepancy can be tracked in the conversion of precursors, which follows the  $E_{cum}$  values. It can be concluded that the  $E_b$  necessary for the formation of BaTiO<sub>3</sub> perovskite is available, but most of it is still lost during grinding (in the form of heat or friction). For this reason, the corrective effect of  $E_{cum}$  is necessary, which counteracts this relatively low  $E_b$ . For this reason, the conversion of starting materials follows the course of  $E_{cum}$ .

In contrast, in the case of samples (TC300/25, FN500/10, TC400/10) framed by a dashed line (Figure 5), the values of  $E_{cum}$  are close to each other, with the largest difference being less than 5%. The  $E_b$  values are as follows: 0.0845; 0.132; 0.157 J/hit. The difference relative to the maximum value (TC400/10) is 46.2% for TC300/25 and 16.0% for FN500/10 samples. But the difference in the conversion of the starting materials is 28.6% for the TC300/25 and only 4.8% for the FN500/10 sample. From this, it can be concluded that, under the circumstances, further increases in the  $E_b$  will no longer bring such a significant increase in the transformation of the precursors. This is confirmed by the fact that, in the case of the TC500/10 compared to the TC400/10 sample, an increase in  $E_b$  by 56.1% and 95.3% in  $E_{cum}$  only causes an increase in conversion by 12%. Based on these results, the two values can be determined from the point of view of both  $E_b$  and the  $E_{cum}$ , between which the perovskite structured BaTiO<sub>3</sub> is formed, and the speed of production can be influenced without compromising the quality of the product.

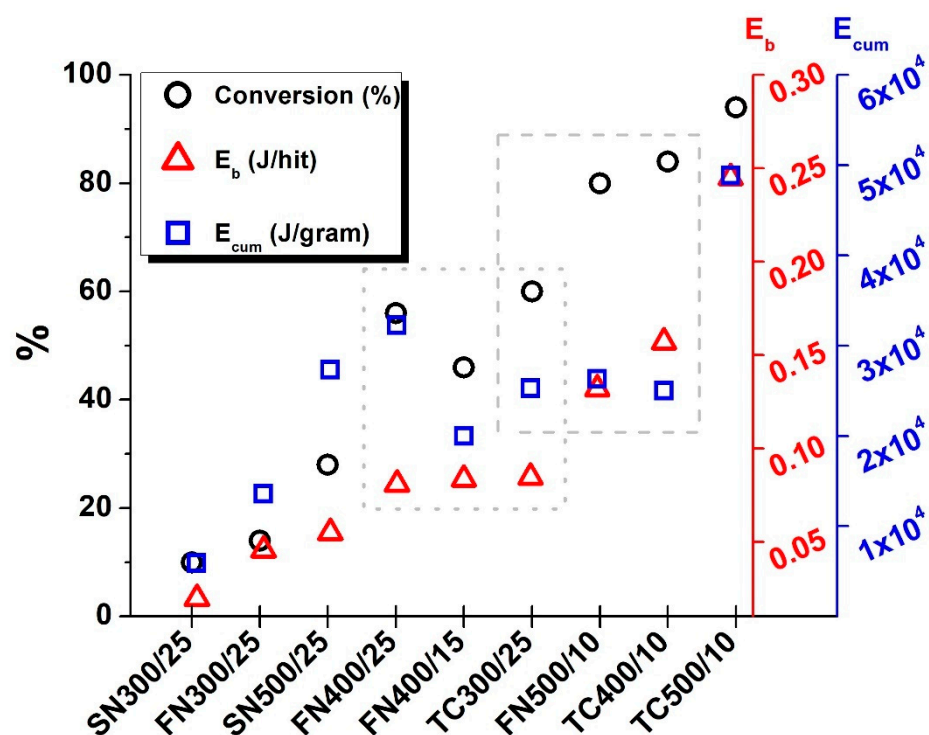


**Figure 5.** The conversion of the precursors (○), the ball-impact ( $E_b$ ,  $\Delta$ ) energy and the cumulative energy ( $E_{cum}$ ,  $\square$ ) in case of all grinding sets. The areas with the dotted and dashed lines show the samples compared in the text.

Figure 6 shows the TEM images of end-product in the case of SN300/25, FN300/25, and TC300/25 samples. By increasing the density of the grinding vessels, the morphology of the particles becomes sharper. While only a mixture of starting materials can be seen in the  $\text{Si}_3\text{N}_4$  grinding vessel (SN300/25), as confirmed by the XRD results, individual particles can be distinguished in the samples made in the FeNi (FN300/25) and TC (TC300/25) grinding vessel. By the TEM images, size distribution histograms were made in the case of FN300/25 and TC300/25 samples. Due to the sufficient  $E_b$ , particle growth is inhibited during the formation of the  $\text{BaTiO}_3$  structure. It follows that, the size of the particles falls within the nano range. The conspicuous difference between the material produced in the two grinding vessels is that the increase in particle size was measurable in the TC vessel, which provides more impact energy ( $E_b$ ). This phenomenon may have been caused by excessive  $E_{cum}$ , which thus led to the sintering of particles. This process is orders of magnitude greater in the case of subsequent heat treatment, while in this case, it allows the final size distribution of the product to be regulated. Overall, the average diameter of the  $\text{BaTiO}_3$  perovskite particles is 13.2 nm (FN300/25) and 19.2 nm (TC300/25).

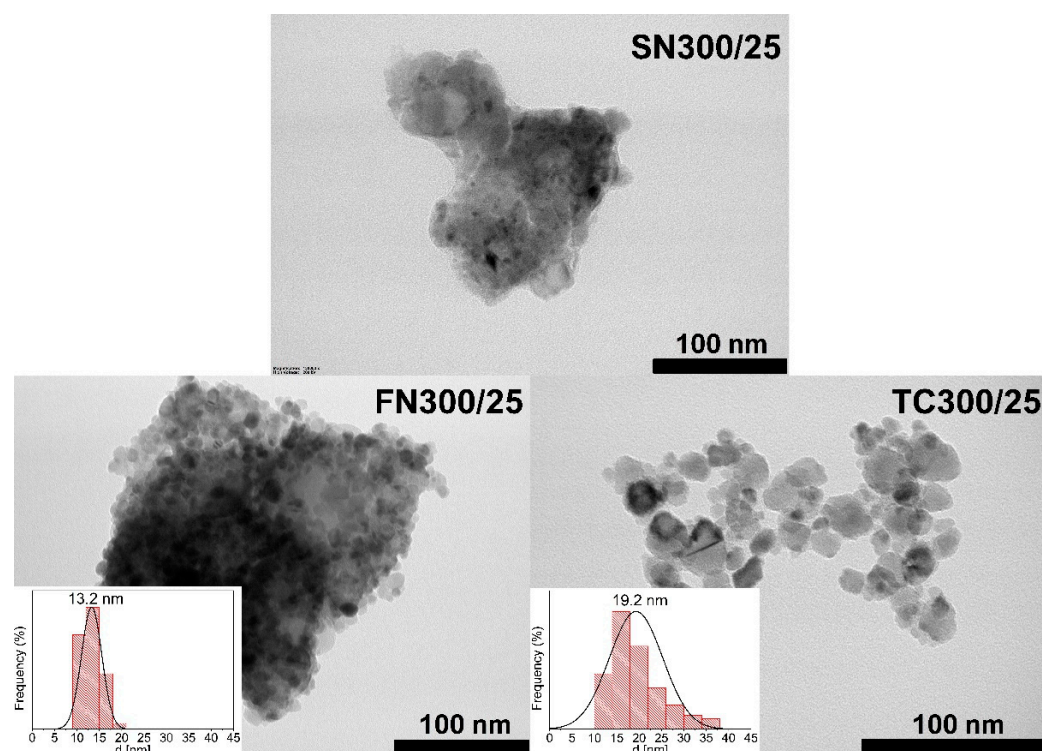


**Figure 6.** TEM images of BaTiO<sub>3</sub> perovskites synthesized in the Si<sub>3</sub>N<sub>4</sub> (SN300/25), FeNi (FN300/25) and TC (TC300/25) grinding vessels.

#### 4. Conclusions

The formation of BaTiO<sub>3</sub> from BaO and TiO<sub>2</sub> was studied in grinding vessels made of different materials, at different rotational speeds and a different number of grinding balls. Based on XRD and Raman measurements, the lowest ball-impact energy ( $E_b$ ) with which perovskite-structured BaTiO<sub>3</sub> can be formed under the studied experimental conditions has been determined ( $E_b = 50$  mJ/hit). Above this value, within a wide range, the transformation of starting materials is almost continuously increasing. It has been shown that to produce the BaTiO<sub>3</sub> perovskite in sufficient quantities, the synchronization of  $E_b$  and cumulative energy ( $E_{cum}$ ) is essential. Based on the results obtained, the highest  $E_b$  value can be determined, which can be used to speed up the formation of the product ( $E_b = 160$  mJ/hit). Above this value, the additional energy no longer contributes to increasing the rate of reaction. This excess energy often causes the product transformation, crystallization, or growth of the individual particles through the process of sintering. In this case, by accurately defining the grinding conditions, the parameters necessary for the transformation have been successfully determined without further transformation of the product. Choosing the necessary  $E_b$  and  $E_{cum}$  allows for the formation of the BaTiO<sub>3</sub> structure, and in addition, increasing these energies, also allows to control of the final size. In addition to the controllability of mechanochemical perovskite-synthesis, the results support the goodness of the model for calculating  $E_b$  and  $E_{cum}$ . This allows the results of the experiments to be quantified, thereby converting the grinding parameters between grinding vessels of different materials or different types of planetary ball mills.

**Author Contributions:** G.K.: Conceptualization, Methodology, Formal analysis, Visualization, Validation, Writing—original draft. K.L.: measurements, laboratory work. C.D.: measurements, formal analysis. A.R.: Writing—review & editing. Á.K.: Supervision, Funding acquisition. Z.K.: Supervision, Funding acquisition. All authors have read and agreed to the published version of the manuscript.

**Funding:** This research was funded by the János Bolyai Research Fellowship of the Hungarian Academy of Sciences (BO/00835/19/7 for G.K. and BO/00384/21/7 for A.R.), and by the professional support of the New National Excellence Program of the Ministry of Innovation and Technology

ÚNKP-21-5-SZTE-547 for G.K. and ÚNKP-21-5-SZTE-876 for A.R. Project No. TKP2021-NVA-19 has been implemented with the support provided by the Ministry of Innovation and Technology of Hungary from the National Research, Development and Innovation Fund, financed under the TKP2021-NVA funding scheme.

**Institutional Review Board Statement:** Not applicable.

**Informed Consent Statement:** Not applicable.

**Data Availability Statement:** Not applicable.

**Conflicts of Interest:** The authors declare that they have no known competing financial interests or personal relationships that could have appeared to influence the work reported in this paper.

## References

1. Vijatovic, M.; Bobic, J.; Stojanovic, B. History and challenges of barium titanate: Part I. *Sci. Sinter.* **2008**, *40*, 155–165. [[CrossRef](#)]
2. Jiang, B.; Iocozzia, J.; Zhao, L.; Zhang, H.; Harn, Y.-W.; Chen, Y.; Lin, Z. Barium titanate at the nanoscale: Controlled synthesis and dielectric and ferroelectric properties. *Chem. Soc. Rev.* **2019**, *48*, 1194–1228. [[CrossRef](#)] [[PubMed](#)]
3. Cinčić, D.; Brekalo, I.; Kaitner, B. Effect of atmosphere on solid-state amine–aldehyde condensations: Gas-phase catalysts for solid-state transformations. *Chem. Commun.* **2012**, *48*, 11683–11685. [[CrossRef](#)]
4. Stolar, T.; Užarević, K. Mechanochemistry: An efficient and versatile toolbox for synthesis, transformation, and functionalization of porous metal–organic frameworks. *CrystEngComm* **2020**, *22*, 4511–4525. [[CrossRef](#)]
5. Tan, D.; Loots, L.; Friščić, T. Towards medicinal mechanochemistry: Evolution of milling from pharmaceutical solid form screening to the synthesis of active pharmaceutical ingredients (APIs). *Chem. Commun.* **2016**, *52*, 7760–7781. [[CrossRef](#)] [[PubMed](#)]
6. Stojanović, B.D.; Jovalekić, C.; Vukotic, V.; Simoes, A.Z.; Varela, J.A. Ferroelectric Properties of Mechanically Synthesized Nanosized Barium Titanate. *Ferroelectrics* **2005**, *319*, 65–73. [[CrossRef](#)]
7. Stojanovic, B.; Simoes, A.; Paiva-Santos, C.; Jovalekic, C.; Mitic, V.; Varela, J. Mechanochemical synthesis of barium titanate. *J. Eur. Ceram. Soc.* **2005**, *25*, 1985–1989. [[CrossRef](#)]
8. Garbarz-Glos, B.; Bak, W.; Budziak, A.; Dulian, P.; Lisinka-Czekaj, A.; Czekaj, D. The application of the mechanochemical synthesis for the preparation of advanced ceramics based on barium titanate. *Arch. Metall. Mater.* **2020**, *65*, 1391–1396.
9. van Hal, H.; Groen, W.; Maassen, S.; Keur, W. Mechanochemical synthesis of BaTiO<sub>3</sub>, Bi<sub>0.5</sub>Na<sub>0.5</sub>TiO<sub>3</sub> and Ba<sub>2</sub>NaNb<sub>5</sub>O<sub>15</sub> dielectric ceramics. *J. Eur. Ceram. Soc.* **2001**, *21*, 1689–1692. [[CrossRef](#)]
10. Aydin, Z.; Turgut, S.; Akbas, H.Z. Structural Differences of BaTiO<sub>3</sub> Ceramics Modified by Ultrasonic and Mechanochemical Methods. *Sov. Powder Met. Met. Ceram.* **2018**, *57*, 490–497. [[CrossRef](#)]
11. Jost, W. *Fast Reactions in Solids, von FP Bowden und AD Yoffe*; Butterworths Scientific Publications: London, UK, 1958; Volume 71, p. 752.
12. Weichert, R.; Schönert, K. On the temperature rise at the tip of a fast running crack. *J. Mech. Phys. Solids* **1974**, *22*, 127–133. [[CrossRef](#)]
13. Gomes, M.A.; Lima, A.; Eguiluz, K.; Salazar-Banda, G.R. Wet chemical synthesis of rare earth-doped barium titanate nanoparticles. *J. Mater. Sci.* **2016**, *51*, 4709–4727. [[CrossRef](#)]
14. Seo, K.W.; Kong, H.G. Hydrothermal preparation of BaTiO<sub>3</sub> thin films. *Korean J. Chem. Eng.* **2000**, *17*, 428–432. [[CrossRef](#)]
15. Sun, W.; Li, C.; Li, J.; Liu, W. Microwave-hydrothermal synthesis of tetragonal BaTiO<sub>3</sub> under various conditions. *Mater. Chem. Phys.* **2006**, *97*, 481–487. [[CrossRef](#)]
16. Catauro, M.; Tranquillo, E.; Poggetto, G.D.; Naviglio, S.; Barrino, F. Antibacterial Properties of Sol–Gel Biomaterials with Different Percentages of PEG or PCL. *Macromol. Symp.* **2020**, *389*, 1900056. [[CrossRef](#)]
17. Šagud, I.; Zanolla, D.; Perissutti, B.; Passerini, N.; Škorić, I. Identification of degradation products of praziquantel during the mechanochemical activation. *J. Pharm. Biomed. Anal.* **2018**, *159*, 291–295. [[CrossRef](#)]
18. Burgio, N.; Iasonna, A.; Magini, M.; Martelli, S.; Padella, F. Mechanical Alloying of the Fe–Zr System—Correlation between Input Energy and End-Products. *Il Nuovo Cimento D* **1991**, *13*, 459–476. [[CrossRef](#)]
19. Kozma, G.; Puskás, R.; Papp, I.; Béteky, P.; Kónya, Z.; Kukovecz, Á. Experimental validation of the Burgio–Rojac model of planetary ball milling by the length control of multiwall carbon nanotubes. *Carbon* **2016**, *105*, 615–621. [[CrossRef](#)]
20. Andonova, S.M.; Senturk, G.S.; Kayhan, E.; Ozensoy, E. Nature of the Ti–Ba Interactions on the BaO/TiO<sub>2</sub>/Al<sub>2</sub>O<sub>3</sub> NO<sub>x</sub> Storage System. *J. Phys. Chem. C* **2009**, *113*, 11014–11026. [[CrossRef](#)]
21. Zhang, W.F.; He, Y.L.; Zhang, M.S.; Yin, Z.; Chen, Q. Raman scattering study on anatase TiO<sub>2</sub> nanocrystals. *J. Phys. D–Appl. Phys.* **2000**, *33*, 912–916. [[CrossRef](#)]
22. Venkateswaran, U.D.; Naik, V.M.; Naik, R. High-pressure Raman studies of polycrystalline BaTiO<sub>3</sub>. *Phys. Rev. B* **1998**, *58*, 14256–14260. [[CrossRef](#)]
23. Shiratori, Y.; Pithan, C.; Dornseiffer, J.; Waser, R. Raman scattering studies on nanocrystalline BaTiO<sub>3</sub> Part I—Isolated particles and aggregates. *J. Raman Spectrosc.* **2007**, *38*, 1288–1299. [[CrossRef](#)]
24. Hayashi, H.; Nakamura, T.; Ebina, T. In-situ Raman spectroscopy of BaTiO<sub>3</sub> particles for tetragonal–cubic transformation. *J. Phys. Chem. Solids* **2013**, *74*, 957–962. [[CrossRef](#)]

25. Lazarevic, Z.; Romčević, N.; Vijatović, M.; Paunović, N.; Romčević, M.; Stojanović, B.; Dohčević-Mitrović, Z. Characterization of Barium Titanate Ceramic Powders by Raman Spectroscopy. *Acta Phys. Pol. A* **2009**, *115*, 808–810. [[CrossRef](#)]
26. Sydoruk, V.; Zazhigalov, V.A.; Khalameida, S.; Wiczorek-Ciurowa, K. Mechanochemical synthesis of BaTiO<sub>3</sub> using different forms of TiO<sub>2</sub>. *Inorg. Mater.* **2010**, *46*, 1126–1130. [[CrossRef](#)]
27. Siddheswaran, R.; Šutta, P.; Novák, P.; Netrvalová, M.; Hendrych, A.; Životský, O. In-situ X-ray diffraction studies and magneto-optic Kerr effect on RF sputtered thin films of BaTiO<sub>3</sub> and Co, Nb co-doped BaTiO<sub>3</sub>. *Ceram. Int.* **2016**, *42*, 3882–3887. [[CrossRef](#)]
28. Sun, Q.; Gu, Q.; Zhu, K.; Jin, R.; Liu, J.; Wang, J.; Qiu, J. Crystalline Structure, Defect Chemistry and Room Temperature Colossal Permittivity of Nd-doped Barium Titanate. *Sci. Rep.* **2017**, *7*, 42274. [[CrossRef](#)]
29. Rojac, T.; Kosec, M.; Malič, B.; Holc, J. The application of a milling map in the mechanochemical synthesis of ceramic oxides. *J. Eur. Ceram. Soc.* **2006**, *26*, 3711–3716. [[CrossRef](#)]
30. Magini, M.; Iasonna, A.; Padella, F. Ball milling: An experimental support to the energy transfer evaluated by the collision model. *Scr. Mater.* **1996**, *34*, 13–19. [[CrossRef](#)]
31. Abdellaoui, M.; Gaffet, E. The physics of mechanical alloying in a planetary ball mill: Mathematical treatment. *Acta Met. Mater.* **1995**, *43*, 1087–1098. [[CrossRef](#)]
32. Raja, S.; Bheeman, D.; Rajamani, R.; Pattiyappan, S.; Sugamaram, S.; Bellan, C.S. Synthesis, Characterization and Remedial Aspect of BaTiO<sub>3</sub> Nanoparticles Against Bacteria. *Nanomed. Nanobiol.* **2015**, *2*, 16–20. [[CrossRef](#)]
33. Rosenkranz, S.; Breitung-Faes, S.; Kwade, A. Experimental investigations and modelling of the ball motion in planetary ball mills. *Powder Technol.* **2011**, *212*, 224–230. [[CrossRef](#)]